This article has been accepted for inclusion in a future issue of this journal. Content is final as presented, with the exception of pagination.

Design and Analysis of a Planar Flux-Switching Permanent Magnet Motor

Hong-Jin Hu[1], Guang-Zhong Cao[1], Su-Dan Huang[1], Chao Wu[1], Jin-Chang Guo[1], De-Liang Liang[2], and Rui-Kun Mai[3]

[1]Shenzhen Key Laboratory of Electromagnetic Control, Shenzhen University, Shenzhen 518060, China
[2]State Key Laboratory of Electrical Insulation and Power Equipment, Xi'an Jiaotong University, Xi'an 710049, China
[3]School of Electrical Engineering, Southwest Jiaotong University, Chengdu 611756, China

In this paper, a planar flux-switching permanent magnet (PFSPM) motor, which is the first of its kind for planar motors, is designed and analyzed. First, the topology structure, modeling, and operating principle of the PFSPM motor are clarified. Then, the initial dimension of the PFSPM motor is determined in terms of its topology structure. Based on the initial dimension, the width of the iron core and the length of the permanent magnet are optimized to increase the thrust force and reduce the cogging force. In addition, a 3-D finite-element analysis (FEA) is performed. Finally, the experiments are conducted based on a developed prototype of the PFSPM motor with the optimized dimension. The results demonstrate that the thrust force is increased by 21%, and the cogging force is reduced by 56% via FEA; the thrust force of the experimental measurement is largely consistent with that determined via the FEA.

Index Terms—**Flux-switching permanent magnet (FSPM) motor design, planar motor.**

I. Introduction

PLANAR motors are an attractive positioning device for precision positioning applications, such as semiconductor and microscale manufacturing, due to their simple structure, high precision, low friction, and low cost [1], [2]. Planar permanent magnet synchronous motors (PPMSMs), which are one type of planar motor, have a high efficiency and high thrust force density [3]. However, PPMSMs have an increased cost and a reduced reliability because a vast majority of the material is the permanent magnet (PM) [4]. As another type of planar motor, planar switched reluctance motors (PSRMs) have a low cost and high reliability; however, PSRMs have a low efficiency and low thrust force density [5], [6]. The development of a new type of planar motor that combines the advantages of PPMSMs and PSRMs and exhibits high efficiency, high thrust force density, high reliability, and low cost would be a significant advancement for precision positioning applications.

A new type of stator PM brushless motor, namely, the flux-switching PM (FSPM) motor, has received increasing attention in recent years. Both FSPM motors and PM synchronous motors feature high efficiency and high torque densities [7]. FSPM motors and switched reluctance motors both exhibit simple structures, are low cost and have a high reliability [8], [9]. FSPM motors have been applied to develop linear motors for precision positioning applications [10]. Linear FSPM motors have two main structures: a structure with a mover/stator pole pitch ratio of approximately 1 and a structure with a mover/stator pole pitch ratio of 3 [11]. Linear FSPM motors with a mover/stator pole pitch ratio of 3 exhibit a lower thrust force ripple [11], which is significant for precision positioning applications. Therefore, linear FSPM motors with a mover/stator pole pitch ratio of 3 could be suitable for developing a type of planar motor with high efficiency, high thrust force density, high reliability, and low cost.

This paper proposes a planar FSPM (PFSPM) motor with a mover/stator pole pitch ratio of 3. The remainder of this paper is organized as follows. In Section II, the topology structure, modeling, and operating principle of the proposed PFSPM motor are presented. In Section III, the preliminary design and optimization of the PFSPM motor are presented. In Section IV, the experimental results are presented and discussed. Finally, conclusions are drawn in Section V.

II. Proposed PFSPM Motor

A. Topology Structure

The PFSPM motor can be regarded as a combination of two linear FSPM motors, with one oriented orthogonal to the other. A 3-D schematic and a 2-D cross-sectional view along one direction of the proposed PFSPM motor are shown in Fig. 1(a) and (b), respectively. The moving platform consists of six movers, with three movers responsible for the three phases of one axis of the PFSPM motor.

For the PFSPM motor, the relationships among the mover teeth pitch τ_u, stator pole pitch τ_s, and mover pole pitch τ_m are given as

$$\tau_u = 1.5\tau_s = 0.5\tau_m. \tag{1}$$

The relationship of the distance between the adjacent mover and stator pole pitch τ_s is expressed as

$$\lambda = n\tau_s \pm \frac{\tau_s}{3} \tag{2}$$

Manuscript received March 15, 2018; revised May 25, 2018; accepted June 2, 2018. Corresponding authors: G.-Z. Cao and S.-D. Huang (e-mail: gzcao.01@gmail.com; hsdsudan@szu.edu.cn).

Color versions of one or more of the figures in this paper are available online at http://ieeexplore.ieee.org.

Digital Object Identifier 10.1109/TMAG.2018.2846261

0018-9464 © 2018 IEEE. Personal use is permitted, but republication/redistribution requires IEEE permission.
See http://www.ieee.org/publications_standards/publications/rights/index.html for more information.

This article has been accepted for inclusion in a future issue of this journal. Content is final as presented, with the exception of pagination.

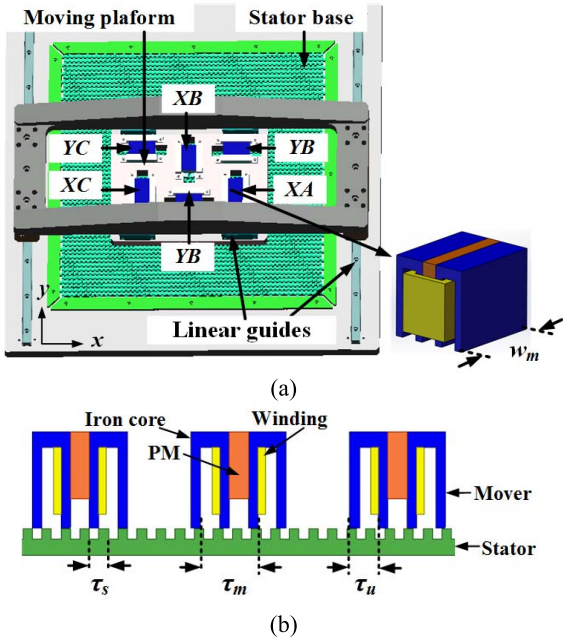

Fig. 1. Overview of the PFSPM motor. (a) 3-D schematic. (b) 2-D cross-sectional view along one direction.

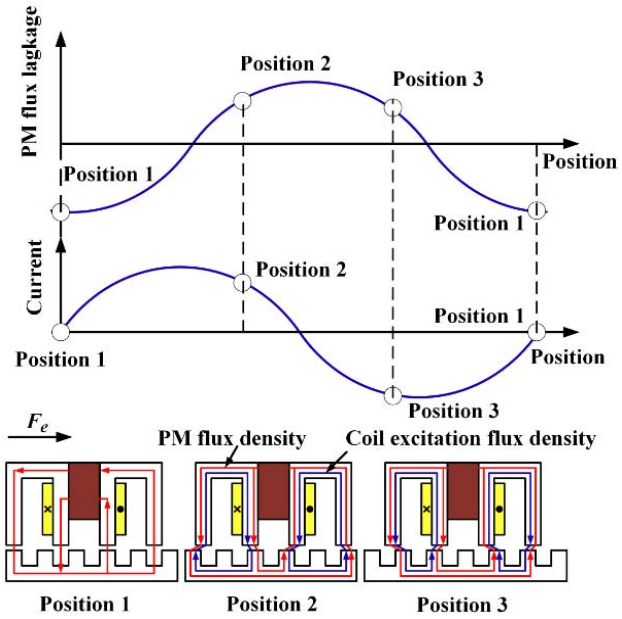

Fig. 2. Operating principle of the PFSPM motor.

where λ is the distance of the adjacent mover, and n is a nonnegative integer.

The thickness of the mover is a multiple of the stator pole pitch, which is given as

$$w_m = k\tau_s \tag{3}$$

where w_m is the thickness of the mover, and k is an integer.

This arrangement allows the total overlap air-gap area to remain unchanged for any perpendicular movement of the platform [12].

TABLE I
INITIAL PARAMETERS OF THE PFSPM MOTOR

Parameter	Description	Value
τ_s	stator pole pitch	7.2 mm
w_{st}	width of the stator teeth	3.6 mm
w_m	thickness of the mover	43.2 mm
τ_m	mover pole pitch	21.6 mm
h_m	high of the mover	36 mm
l_{PM}	length of the PM	26 mm
λ	distance between the adjacent mover	60 mm
B_r	remanence	1.2 T
N	number of turns	150
h_s	height of the stator	10 mm
h_{st}	height of the stator teeth	4 mm
g	air gap length	0.3 mm

B. Modeling

The electromagnetic thrust force of one axis can be expressed as

$$F_{\mathrm{el}} = \sum_{j=a,b,c} F_{\mathrm{elj}} \tag{4}$$

where F_{elj} is the electromagnetic thrust force of j ($j = a, b,$ and c) phase of the l-axis ($l = x, y$), and F_{el} is the electromagnetic thrust force of the l-axis.

For one mover, the electromagnetic thrust force can be obtained from the derivation of the magnetism co-energy [13], which is presented as

$$F_{\mathrm{elj}} = \frac{\partial W_{\mathrm{colj}}}{\partial s} = i_{lj}\frac{d\psi_{\mathrm{PMlj}}}{ds} + \frac{1}{2}i_{lj}^2\frac{dL_{lj}}{ds} - \frac{dW_{\mathrm{PMlj}}}{ds} \tag{5}$$

where s is the position of the mover, W_{colj} is the magnetism co-energy, ψ_{PMlj} is the permanent flux linkage, i_{lj} is the winding current, and W_{PMlj} is the magnetic field energy of the PM. The thrust force is composed of three forces, as presented in the following equation:

$$\begin{cases} F_{\mathrm{PMlj}} = i_{lj}\dfrac{d\psi_{\mathrm{PMlj}}}{ds} \\ F_{\mathrm{rlj}} = \dfrac{1}{2}i_{lj}^2\dfrac{dL_{lj}}{ds} \\ F_{\mathrm{coglj}} = -\dfrac{dW_{\mathrm{PMlj}}}{ds} \end{cases} \tag{6}$$

where F_{PMlj} is the main thrust force produced by the interaction between the winding current and PM flux linkage, F_{rlj} is the reluctance force, and F_{cog} is the cogging force.

C. Operating Principle

The operating principle of the PFSPM motor is presented in Fig. 2. FSPM motors generally have a sinusoidal PM flux linkage. According to (5) and (6), the PFSPM motor must operate at a sinusoidal winding current that has the same phase as the differential of the PM flux linkage to generate a positive thrust force.

This article has been accepted for inclusion in a future issue of this journal. Content is final as presented, with the exception of pagination.

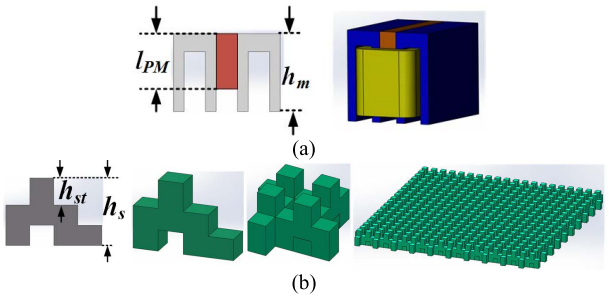

Fig. 3. (a) Mover. (b) Stator.

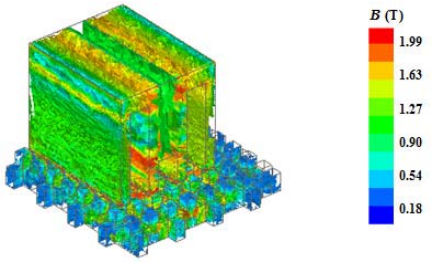

Fig. 4. Flux density distribution of one mover.

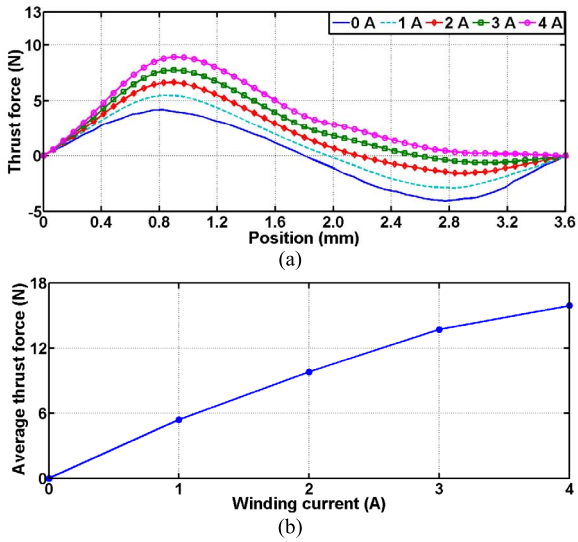

Fig. 5. Thrust force. (a) Thrust force waveform of one mover. (b) Average thrust force of one direction at different winding currents.

III. Motor Design and Optimization

A. Preliminary Design

The initial parameters of the PFSPM motor are listed in Table I. The iron core of the mover is composed of a "U"-shaped silicon steel sheet, as shown in Fig. 3(a). The stator is a network structure constructed from a combination of stator blocks, with each stator block composed of laminated silicon steel, as shown in Fig. 3(b).

The PFSPM motor is analyzed based on the 3-D finite-element analysis (FEA). The flux density distribution of one mover is shown in Fig. 4. The thrust force waveform of one mover at different winding currents is shown in Fig. 5(a). According to (6), when the winding current $ilj = 0$ A, the cogging force is equal to the thrust force. The maximum

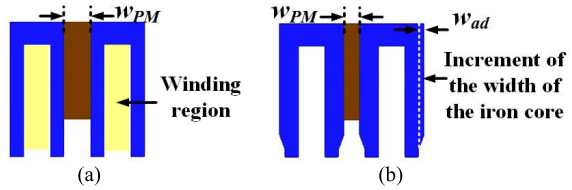

Fig. 6. (a) Mover before optimization. (b) Optimized mover with the increased width of the iron core.

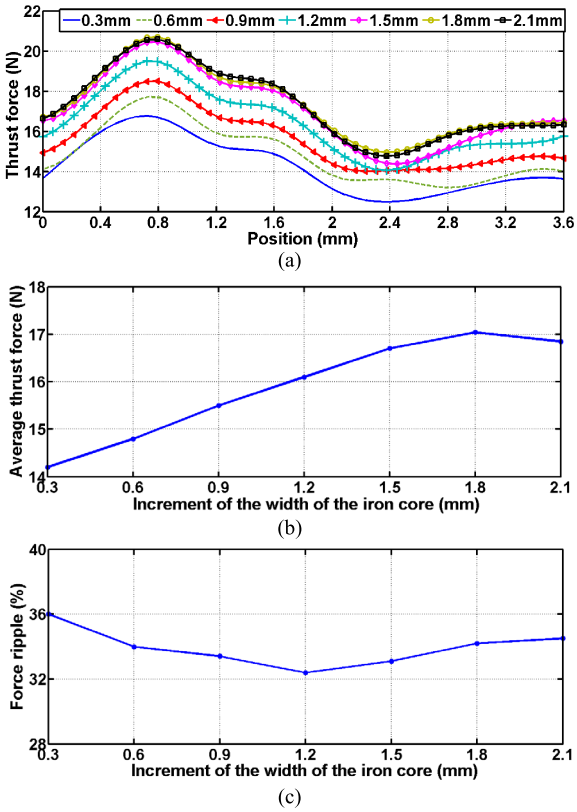

Fig. 7. Influence of the width of the iron core. (a) Thrust force of one direction. (b) Average thrust force of one direction. (c) Force ripple.

cogging force of one mover is 4.1 N. According to (4), the average thrust force of one direction can be calculated as

$$F_{\text{lave}} = \frac{6}{\tau_s} \int_0^{\frac{\tau_s}{2}} F_{ejl} ds. \tag{7}$$

The average thrust force of one direction at different winding currents is shown in Fig. 5(b) and the average thrust force is largely proportional to the winding current.

B. Optimal Design

To obtain better thrust force performance, the optimal design is performed based on 3-D FEA. The optimal objectives of the PFSPM motor design are to increase the thrust force and to reduce the cogging force.

The thrust force can be increased by increasing the air-gap flux density, and the air-gap flux density can be increased by reducing the reluctance of the magnetic circuit. The reluctance of the magnetic circuit consists of the mover reluctance, stator reluctance, and air-gap reluctance. Without considering the

This article has been accepted for inclusion in a future issue of this journal. Content is final as presented, with the exception of pagination.

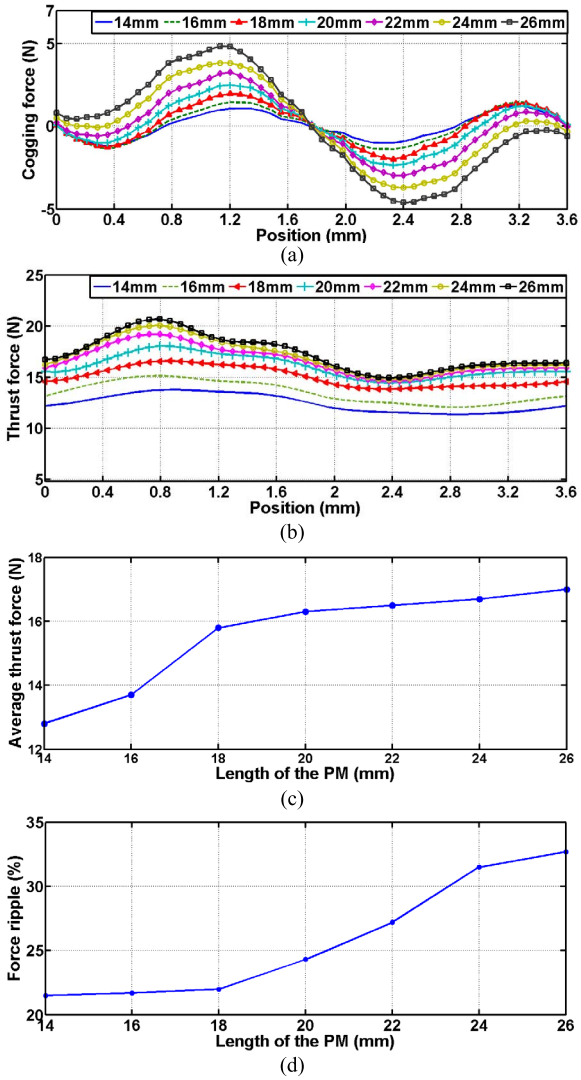

Fig. 8. Influence the length the PM. (a) Cogging force. (b) Thrust force of one direction. (c) Average thrust force of one direction. (d) Force ripple.

changes in the air gap and the stator, the reluctance of the magnetic circuit can be reduced by optimizing the mover.

The reluctance of the mover is expressed as

$$R_m = \frac{L}{\mu_{Fe} S} \tag{8}$$

where R_m is the mover reluctance, S is the cross-sectional area of the iron core, L is the length of the iron core, and μ_{Fe} is the permeability of the iron core materials.

According to (8), R_m can be reduced by increasing the cross-sectional area of the iron core. The cross-sectional area could be increased by increasing the width of the iron core. Fig. 6 shows the mover with the increased width of the iron core. For the installation requirement, the winding region cannot be reduced. When the width of the iron core is increased, the width of the PM would be reduced. The width of the iron core could not be overly increased, because the thrust force would be reduced when the width of the PM is overly reduced. The thrust force and the average thrust force with different w_{ad} at the winding current of 3 A are shown in Fig. 7(a) and (b), respectively, where w_{ad} is the increment of the width of the iron core. The maximum average thrust force appears at $w_{\text{ad}} = 1.8$ mm. The average thrust force is increased by 23%. w_{ad} of 1.8 mm is then chosen.

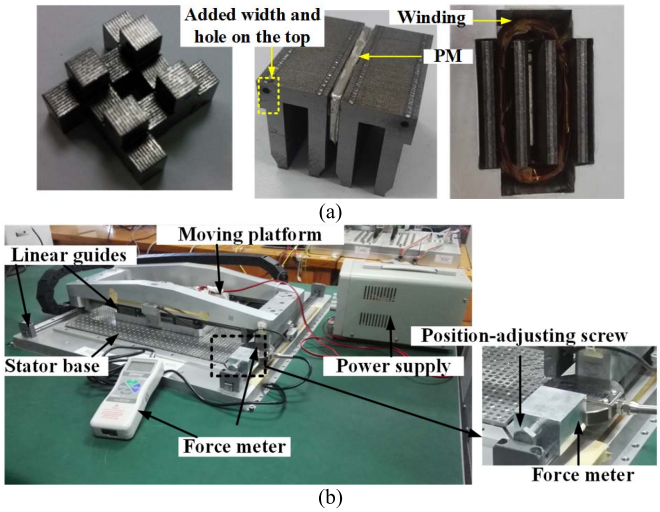

Fig. 9. Developed prototype of the PFSPM. (a) Stator blocks and mover. (b) Experimental setup.

The force ripple is expressed as

$$F_{\text{ripple}} = \frac{F_{\max} - F_{\min}}{F_{\text{ave}}} \times 100\% \tag{9}$$

where $F_{\max}$ is the maximum thrust force of one direction, $F_{\min}$ is the minimum thrust force of one direction, and F_{ave} is the average thrust force of one direction.

The force ripple with different w_{ad} is shown in Fig. 7(c). When $w_{\text{ad}} = 1.8$ mm, the force ripple is 33.2%.

From Fig. 7(a) and (c), the force ripple is the obviously large. The force ripple is mainly caused by the cogging force. To obtain a better thrust force performance, the cogging force needs to be reduced.

The cogging force can be reduced by reducing the length of the PM [14]. The cogging forces of different l_{PM} are shown in Fig. 8(a). The thrust force can be reduced by using a shorter PM. The thrust force waveform and average thrust force of different l_{PM} at a winding current of 3 A are shown in Fig. 8(b) and (c). The cogging force is lower when l_{PM} is reduced; however, the average thrust force is considerably lower when $l_{\text{PM}} < 18$ mm. According to (9), the force ripple with different l_{PM} is presented in Fig. 8(d). Because the cogging force is reduced, the force ripple is reduced. A PM with a length of 18 mm is chosen. The maximum cogging force is 1.8 N. The average thrust force is only 7% lose, and the force ripple is reduced by 11.2%, compared to the PM with l_{PM} of 26 mm.

Based on the above analysis, when a length of PM of 18 mm and w_{ad} of 1.8 mm are used, the maximum cogging force is 56% lower than the initial value, and the average thrust force is increased by 21% compared to the initial value. The thrust force performance is improved through the optimal design.

IV. Experimental Results

The prototype of the PFSPM motor with the optimal dimension is developed. The mover and stator blocks are shown in Fig. 9(a). The actual mover structure has several differences

This article has been accepted for inclusion in a future issue of this journal. Content is final as presented, with the exception of pagination.

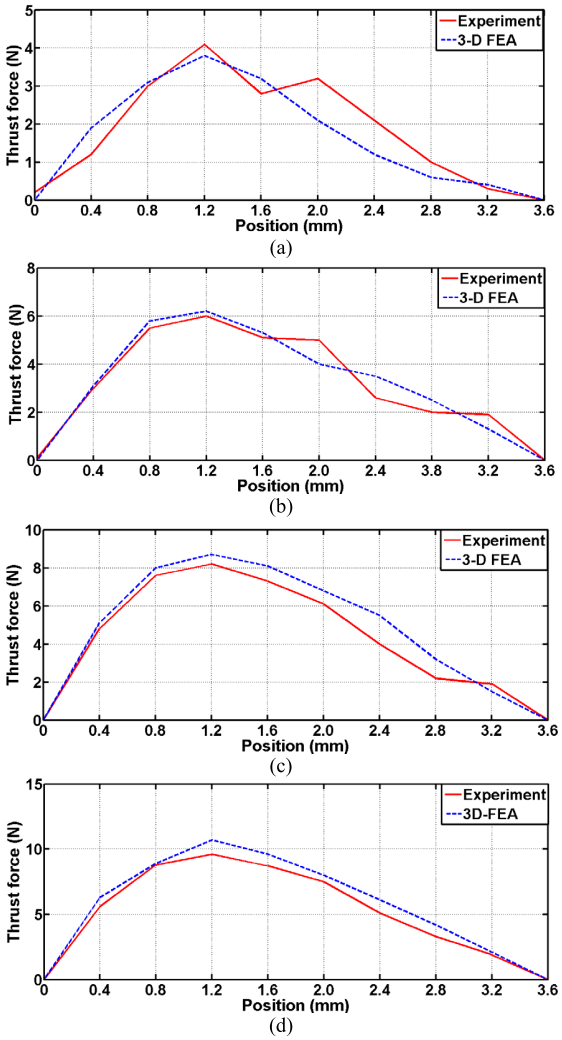

Fig. 10. Results of static thrust force measurement. (a) $i_{lj} = 1$ A. (b) $i_{lj} = 2$ A. (c) $i_{lj} = 3$ A. (d) $i_{lj} = 4$ A.

compared to the mover structure of the FEA. The added width and hole on top of the mover are manufactured to satisfy the installation requirement.

To verify the effectiveness of the PFSPM motor, the static force is measured using a force meter. As shown in Fig. 9(b), the experimental setup consists of a force meter, a position-adjustment screw, and a power supply. The position of the moving platform is adjusted by using a screw. Contact with the force meter and the moving platform. The measurement accuracy of the force meter is 0.1 N. The measurement results of the static force at different winding currents are shown in Fig. 10. The measurement results are disturbed by static friction, which cause inaccurate measurements at certain positions. However, overall, the static force measurement results are largely consistent with the FEA results. According to (4) and (9), the force ripple of the measured thrust force can be calculated. The force ripple with different winding currents is shown in Fig. 11. When the winding current is small, the measured results suffer from a large disturbance due to the static friction, and thus the force ripple of the measured thrust force is much different from the FEA results. Nonetheless, when the winding current is increased, the experimental force ripple largely matches the force ripple of the FEA results.

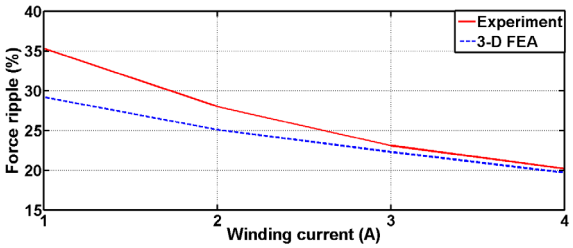

Fig. 11. Force ripple of the measured thrust force.

V. Conclusion

In this paper, a new type of planar motor, named as PFSPM motor, was proposed. The topology structure of the motor was presented, the optimal design of the motor was performed, and the prototype of the PFSPM motor was developed with the optimal structure by the laboratory. The FEA results demonstrate that the thrust force is increased and the cogging force is reduced for the optimal design. The experimental results show that the measured thrust force largely matches to the thrust force determined by the FEA. The effectiveness of the proposed PFSPM motor is verified through the FEA and experimental results. The proposed PFSPM motor featuring high efficiency, high thrust force density, high reliability, and low cost is appropriate for precision positioning applications.

Acknowledgment

This work was supported in part by the National Natural Science Foundation of China under Grant 51677120 and Grant 51275312, in part by the Natural Science Foundation of Guangdong Province, China under Grant 2017A030310460, in part by the Shenzhen Government Fund under Grant KJYY20160428170944786 and Grant JCYJ20160520175515548, and in part by the Fundamental Research Funds for the Shenzhen University under Grant 2017039. Guang-Zhong Cao and Su-Dan Huang contributed equally to this work.

References

[1] C. Hu, Z. Wang, Y. Zhu, M. Zhang, and H. Liu, "Performance-oriented precision LARC tracking motion control of a magnetically levitated planar motor with comparative experiments," *IEEE Trans. Ind. Electron.*, vol. 63, no. 9, pp. 5763–5773, Sep. 2016.

[2] T. Huang, K. Yang, C. Hu, Y. Zhu, and M. Li, "Integrated robust tracking controller design for a developed precision planar motor with equivalent disturbances," *IET Control Theory Appl.*, vol. 10, no. 9, pp. 1009–1017, May 2016.

[3] I.-U.-R. Usman and X. Lu, "Force ripple attenuation of 6-DOF direct drive permanent magnet planar levitating synchronous motors," *IEEE Trans. Magn.*, vol. 51, no. 12, Dec. 2015, Art. no. 8208708.

[4] J. M. M. Rovers, J. W. Jansen, and E. A. Lomonova, "Multiphysical analysis of moving-magnet planar motor topologies," *IEEE Trans. Magn.*, vol. 49, no. 12, pp. 5730–5741, Dec. 2013.

[5] S.-D. Huang *et al.*, "Maximum-force-per-ampere strategy of current distribution for efficiency improvement in planar switched reluctance motors," *IEEE Trans. Ind. Electron.*, vol. 63, no. 3, pp. 1665–1675, Mar. 2016.

[6] G. Z. Cao, J. L. Fang, S. D. Huang, J. A. Duan, and J. F. Pan, "Optimization design of the planar switched reluctance motor on electromagnetic force ripple minimization," *IEEE Trans. Magn.*, vol. 50, no. 11, pp. 1–4, Nov. 2014.

This article has been accepted for inclusion in a future issue of this journal. Content is final as presented, with the exception of pagination.

[7] M. Cheng, W. Hua, J. Zhang, and W. Zhao, "Overview of stator permanent magnet brushless machines," *IEEE Trans. Ind. Electron.*, vol. 58, no. 11, pp. 5087–5101, Nov. 2011.

[8] C. H. T. Lee, J. L. Kirtley, and M. Angle, "A partitioned-stator flux-switching permanent-magnet machine with mechanical flux adjusters for hybrid electric vehicles," *IEEE Trans. Magn.*, vol. 53, no. 11, Nov. 2017, Art. no. 3000807.

[9] J. D. McFarland, T. M. Jahns, and A. M. El-Refaie, "Analysis of the torque production mechanism for flux-switching permanent-magnet machines," *IEEE Trans. Ind. Appl.*, vol. 51, no. 4, pp. 3041–3049, Jul./Aug. 2015.

[10] H. Lin and J. A. Heilig, "Linear hybrid brushless servo motor," U.S. Patent 7 230 355, Jun. 12, 2007.

[11] R. Cao, M. Cheng, and W. Hua, "Investigation and general design principle of a new series of complementary and modular linear FSPM motors," *IEEE Trans. Ind. Electron.*, vol. 60, no. 12, pp. 5436–5446, Dec. 2013.

[12] J. Pan, N. C. Cheung, and J. Yang, "High-precision position control of a novel planar switched reluctance motor," *IEEE Trans. Ind. Electron.*, vol. 52, no. 6, pp. 1644–1652, Dec. 2005.

[13] B. Duiixiri and Z. Qionghua, "A novel single phase doubly salient permanent magnet motor," in *Proc. Int. Conf. Power Electron. Drive Syst.*, Jul. 1999, pp. 725–729.

[14] G. Chun, J. Wu, M. Shen, W. Kong, Y. Hu, and W. Cao, "Investigation of short permanent magnet and stator flux bridge effects on cogging torque mitigation in FSPM machines," *IEEE Trans. Energy Convers.*, vol. 33, no. 2, pp. 845–855, Jun. 2018.